HHS Public Access

Author manuscript

IEEE Trans Biomed Eng. Author manuscript; available in PMC 2020 July 01.

Published in final edited form as:

IEEE Trans Biomed Eng. 2020 July ; 67(7): 2084–2093. doi:10.1109/TBME.2019.2954524.

Miniaturized Intracavitary Forward-Looking Ultrasound Transducer for Tissue Ablation

Howuk Kim, **Huaiyu Wu**

Department of Mechanical and Aerospace Engineering, North Carolina State University, Raleigh, NC 27695, USA.

Namwoo Cho,

Department of Material Science and Engineering, North Carolina State University.

Pei Zhong,

Department of Mechanical Engineering and Material Sciences, Duke University, Durham, NC 27710, USA.

Kamran Mahmood,

Department of Medicine, Division of Pulmonary, Allergy and Critical Care, Duke University.

Herbert Kim Lyerly,

Department of Surgery, Duke University.

Xiaoning Jiang

Department of Mechanical and Aerospace Engineering, North Carolina State University, Raleigh, NC 27695, USA.

Abstract

Objective: This paper aims to develop a miniaturized forward-looking ultrasound transducer for intracavitary tissue ablation, which can be used through an endoscopic device. The internal ultrasound (US) delivery is capable of directly interacting with the target tumor, resolving adverse issues of currently available US devices, such as unintended tissue damage and insufficient delivery of acoustic power.

Methods: To transmit a high acoustic pressure from a small aperture (<3 mm), a double layer transducer (1.3 MHz) was designed and fabricated based on numerical simulations. The electric impedance and the acoustic pressure of the actual device was characterized with an impedance analyzer and a hydrophone. Ex vivo tissue ablation tests and temperature monitoring were then conducted with porcine livers.

Results: The acoustic intensity of the transducer was 37.1 W/cm^2 under 250 V_{pp} and 20% duty cycle. The tissue temperature was elevated to 51.8°C with a 67 Hz pulse-repetition frequency. The temperature profile in the tissue indicated that ultrasound energy was effectively absorbed inside

xjing5@ncsu.edu.

the tissue. During a 5-min sonification, an approximate tissue volume of 2.5 × 2.5 × 1.0 mm^3 was ablated, resulting in an irreversible lesion.

Conclusion: This miniaturized US transducer is a promising medical option for the precise tissue ablation, which can reduce the risk of unintended tissue damage found in noninvasive US treatments.

Significance: Having a small aperture (2 mm), the intracavitary device is capable of ablating a bio tissue in 5 min with a relatively low electric power (< 17 W).

Index Terms—

Tissue ablation; intracavitary transducer; ultrasound therapy; hyperthermia; small aperture

I. Introduction

Ultrasound (US) therapy is an emerging therapeutic modality for cancer that delivers a relatively high acoustic power, in the form of ultrasound waves, to a target inside the body [1]. Focused US has shown its therapeutic possibilities in various cancers and malignant tumors of liver, breast, pancreas, and prostate. [2][3][4]. US waves, technically, result in the vibration of molecules in the target tissue, which causes frictional heat [5][6]. Due to the heat energy, the temperature of the tissue can be elevated to over 60°C, resulting in the coagulative necrosis of the tissue [7][8][9].

However, focused US is currently delivered clinically by a surface probe [10][11]. The noninvasive approach needs careful attention to avoid unintended damage to healthy tissues. In addition, the current US device requires high power (> 100 W) to deliver the sufficient acoustic power into the target region that is deep inside the body [12]. This approach is not feasible for organs deep in the body, such as the lungs. In contrast, a minimally invasive US delivery system, inserted through a bronchoscope into the lung, can mitigate these issues by directly interacting with the target tissue. Direct sonification can focus the acoustic power more accurately to the lesion and transfer a relatively high acoustic energy with a relatively low electric input power (< 17 W) from the device. Despite perspective advantages, studies on intracavitary US transducer for tissue ablation application has been lacking due to its small aperture size and difficulty in fabrication.

Besides US energy, various intracavitary or endoscopic modalities were investigated for tissue ablation in the past, such as radio frequency (RF), microwave (MW), and cryoablation (CA) [13]. Existing methods, however, still restrict common medical applications due to adverse effects and inefficacy. For instance, RF ablation can cause excessive damage to normal tissue and vascular fistulae [14][15]. Meanwhile, it is relatively hard to control the ablating zone precisely with the MW method, and it needs to resolve the heating issue of the coaxial cable and the connecting shaft [16][17]. The CA approach is not free from complications, such as fistulae to surrounding structures [18][19]. In addition, the performance of CA may be greatly degraded by a high blood flow [20]. In contrast, US-assisted ablation is relatively safe and reliable; as long as US waves are directed and focused precisely to the lesion, no significant degree of negative effects are seen on the surrounding

tissue [21][22], making US safer than currently available modalities. Moreover, there are less technical challenges with US compared to other modalities, such as RF ablation, including selection of electrode shape and grounding pad placement.

Catheter-guided intracavitary US transducers have recently attracted much attention for some therapeutic applications, such as thrombolysis, drug delivery, and tissue ablation [23–26]. Many interstitial tissue ablating devices are currently side-looking applicators using either tubular or planar active elements [27][28][29]. The side-looking transducers are more advantageous to maximize the aperture surface and accordingly target volume compared to forward-looking transducers [30]. The side-looking transducers with cylindrical active elements transmit US waves evenly about the circumferential direction [28][31][32], yet it is relatively hard for them to produce deep thermal lesions than their planar counterparts [27,30,33]. Prat et al. reported a side-looking plane actuator using a single piezoelectric plate, yet acoustic intensity was about 14 W/cm^2 [34]. Makin et al. reported plane phased array transducers, but a relatively complicated control system for beamforming was required [35]. Meininger et al. proposed an interstitial US device utilizing a gas-filled reflector which directs the focused US waves from the side to the forward direction [36]; however, there is still a potential loss of acoustic energy due to the reflector. In 2015, Li et al. reported an endoscopic high-intensity focused US device and validated its performance in an in vivo porcine model [37]. The aperture size of their device was about 12 mm and required an electric power of 150 W to ablate the target tissue [37]. In [26], a multilayered US device was developed to transfer a relatively high acoustic power along the forward direction to activate the inertial cavitation in a thrombus. Nonetheless, the short focal distance (< ~1 mm) restricts its practical application for tissue ablation. Hence, a novel intracavitary transducer, having a small aperture size (< 3 mm), needs to be developed for the delivery of sufficient acoustic intensity (> 10 W/cm^2) to a relatively far distance (> 2 mm).

The objective of this paper is to develop a miniaturized forward-looking US transducer capable of transmitting a relatively high acoustic power from a small aperture to ablate a target tissue (Fig. 1). The contents of this paper are organized as follows: First, the temperature elevation of the focused US is estimated using the bio-heat transfer equation. Second, the US transducer was designed and numerically simulated by using a commercial software. Third, based on the simulation results, the miniaturized transducer was fabricated and characterized. Finally, the performance of the transducer was demonstrated through ex vivo tests using porcine livers.

II. Materials and Methods

A. Theoretical Prediction

Tissue ablation refers to the conversion of acoustic energy into heat energy, leading to coagulative necrosis of targeted tissue. For accurate ablation with minimized damage to healthy tissue, it is essential to determine the proper degree of the US energy absorbed inside the tissue as well as the operating condition of the US device. Hence, the theoretical prediction of the temperature elevation during sonification needs to be estimated to provide the reference operating condition of the US transducer. The bio-heat transfer equation for this analysis is expressed as [38–40]

$$\dot{T} = K\nabla^2 T/c_v + q_v/c_v - T/\tau \tag{1}$$

where q_v is the heat source function, T is the temperature rise above that of blood; K is the thermal conductivity, τ is the time constant for perfusion, and c_v is the volume specific heat for tissue. The perfusion time constant can be determined by [41]

$$\tau = \rho_b c_v/(wc_b) \tag{2}$$

where ρ_b is the density of the blood, c_b is the volume specific heat for blood, and w is the blood perfusion rate. The time constant is inversely proportional to the blood perfusion rate [40].

A point source solution in an infinitesimal volume (dV) is computed by using the Green function as [40]

$$dT = \frac{C}{r}\left\{\exp\left(\frac{-r}{L}\right)\left[2 - \operatorname{erfc}\left(\sqrt{\frac{t}{\tau}} - \frac{r}{\sqrt{4\kappa t}}\right)\right] + \frac{1}{\exp(-r/L)}\operatorname{erfc}\left(\sqrt{\frac{t}{\tau}} + \frac{r}{\sqrt{4\kappa t}}\right)\right\} \tag{3}$$

and

$$C = \frac{q_v}{8\pi K}dV, r = \sqrt{x^2 + y^2 + z^2}, \text{ and } L = \sqrt{\kappa\tau} \tag{4}$$

where the thermal diffusivity κ is given by K/c_v, x and y are the lateral coordinates, z is the axial coordinate, and t indicates the time. The blood perfusion rate is excluded in this study; thus, (3) is simplified as

$$T = \frac{2C}{r}\operatorname{erfc}\left(\frac{r}{\sqrt{4\kappa t}}\right) \tag{5}$$

The volume rate of heat generation q_v due to US absorption is given by [42]

$$q_v = 2\alpha I \tag{6}$$

where I is the acoustic intensity, and α is the attenuation coefficient. Here, near-field complications are neglected, and the acoustic beam is projected as a column, with the same sectional area as the transducer surface. Finally, temperature elevation in the tissue volume is predicted by integrating the point-source solution of (3) with respect to x, y, and z. Table I tabulates the parametric values for the theoretical prediction.

In addition to temperature prediction, the thermal necrosis of the tissue can be quantitatively assessed using the Sapareto and Dewey criteria [45]. The equivalent minutes at 43°C (EM_{43}) is defined as

$$EM_{43}(x, y, z, t) = \int_0^{t_4} R^{43 - T(x, y, z, t)}dt, \tag{7a}$$

$$R = \begin{cases} 0 & T < 37°C \\ 0.25 & 37°\text{C} \le T < 43°\text{C} \\ 0.5 & T \ge 43°\text{C} \end{cases} \quad (7b)$$

where t_d indicates the total treatment duration. Notably, majority of the tissue dies upon exposure to a thermal dose of EM_{43} = 240 min [46]. Accordingly, the thermal necrosis criteria are interpreted as a threshold when the coagulative necrosis results in [46].

B. Transducer Design

Several aspects are addressed to design the miniaturized US transducer – material type, number of active layers, backing material, matching layer, and bonding media. First, PZT-5A was chosen for the active layer due to its higher piezoelectric constants compared with hard PZT materials, such as PZT-4 or PZT-8, and its stronger mechanical strength compared with soft PZT material, such as PZT-5H [47]. Second, double active layers with 500 μm thickness were stacked together. The main advantage of stacking active layers is that it enables the transmission of a relatively high acoustic power with a relatively low electric voltage input by lowering the electric impedance level at the operating frequency. Third, an air-backing is adopted to transmit the acoustic pressure output along the forward-direction of the transducer. The acoustic impedance of the backing media is about 500 Rayls, which is much lower than that of the active element (~34 MRayls) [48][49]. Fourth, a matching layer, the thickness of which is determined by the quarter wavelength, was integrated with the stack layer to intensify the resulting acoustic pressure. Fifth, a conductive epoxy resin was used as bonding material. Material properties of the double layer transducer are listed in Table II. Fig. 2 presents the schematic expression of the designed double layer transducer.

C. Numerical Simulation

The performance of the designed model was predicted by using a commercial finite element analysis (FEA) software (Release 17.1, ANSYS, Inc., Canonsburg, PA, USA). Fig. 3 illustrates the boundary conditions of the FEA simulation. The fluid-structure interaction boundary was assigned between the acoustic (i.e., water medium) and the structure (i.e., transducer parts) meshes. Radiation condition (i.e., no reflection) was applied onto the outer surface of the acoustic medium. The backing layer was replaced by the acoustic impedance boundary condition. In addition, a quarter model was used to reduce the computational burden. For the computation, the harmonic response was used for the electric impedance response of the transducer, with frequency span from 5 kHz to 2 MHz. A unit electric voltage level was assigned to the positive electrode surfaces, whereas the ground surfaces had zero voltage. After the electric impedance simulation, the acoustic field was simulated with the operating frequency obtained. Table II outlines the material properties used in the simulation.

D. Transducer Fabrication

The double-layer US transducer was fabricated based on the mechanical design and the simulation results. Fig. 4 illustrates the manufacturing process of the transducer. First, two PZT-5A layers were bonded together with a conductive epoxy resin (E-Solder 3021, Von-

Roll Inc., Cleveland, OH). Second, a matching layer was prepared with the mixture of epoxy resin (EPO-TEK 301, Epoxy tech. Inc., Billerica, MA) and Al_2O_3 powder. The matching layer was attached on the top surface of the PZT stack. Third, the stack was diced into 2 mm by 2 mm pieces (DAD323, Disco Corp., Tokyo, Japan). Fourth, coaxial cable (RG174U, Olympic Wire & Cable Corp., Fairfield, NJ) was connected on the sliced stack, using the E-solder. Parylene-C layer, 50 μm thick, was used on the wire connection for electric insulation. Fifth, the backing layer composed of air-bubble powder (i.e., provided by Blatek Industries Inc., State College, PA) and epoxy resin (EPO-TEK 301, Epoxy Tech. Inc., Billerica, MA) was deposited at the rear surface of the stack, with a thickness of about 1.5 mm. Meanwhile, the air-bubble powder was mixed with the epoxy resin, with a volume ratio of 3:1. Shaking the mixture at 10,000 rpm using a centrifuge (Microfuge Lite, Beckman Coulter, Brea, CA) for 7 min, most bubble powders moved to the upper region of the mixture due to their relatively light weight. As such, only the portion 20% of the height from the top surface of the mixture was used for the deposition of the backing layer. After the deposition of the backing layer on the transducer, it was cured in 40°C for 3 hours. The acoustic impedance of the backing layer is known to be about 500 Rayls [48]. Finally, the transducer was coated by a 10-μm thick Parylene-C layer to make it waterproof. Fig. 5 shows the fabricated transducer.

E. Transducer Characterization

The electric impedance response of the transducer was measured in the frequency band from 5 kHz to 2 MHz by using an impedance analyzer (4294A, Agilent Tech. Inc., Santa Clara, CA). The actual response was compared with the prediction from the FEA simulation. The required electric power for the transducer was estimated using the following formula:

$$P_{avg} = \eta \frac{1}{1-\zeta} \frac{V_{eff}^2}{Z} \tag{8}$$

where η is the duty cycle, ζ is the reflection coefficient due to the electric mismatch, Z is the impedance of the transducer, and V_{eff} is the effective input voltage. Confirming the impedance response and the power of the transducer, the acoustic pressure output was measured through the hydrophone test (Fig. 6). The function generator (33250A, Agilent Tech. Inc., Santa Clara, CA) produced a sinusoidal pulse of 10 cycles per 10 ms and sent to the power amplifier (75A250A, AR, Souderton, PA). The amplified signal was fed into the US transducer, and the acoustic pressure output was measured with a hydrophone (HGL-0085, ONDA Corp., Sunnyvale, CA). Acoustic intensity was estimated based on the acoustic pressure result.

F. Ex Vivo Test

The ex vivo test was conducted to determine the temperature elevation of a biologic tissue upon sonification and to demonstrate the therapeutic efficacy of the miniaturized US forward-looking transducer. Fig. 7(a) shows the test set-up. A fresh porcine liver was prepared from a butcher's shop. It was sliced into a small piece, about 30 mm × 30 mm × 6 mm, and was placed on the bottom of a plastic water bath. The bath was filled with water at 37°C. The US transducer was operated with 1.3 MHz under 20% duty cycle and 250 V_{pp}

magnitude. The steady state temperature was subsequently controlled by changing the pulse-repetition frequency.

The temperature elevation of the ablated portion was measured by using a needle-type thermocouple (HYP0, Omega Engineering Inc., Norwark, CT). The insertion of the thermocouple did not significantly distort the acoustic field in the liver since the thermocouple diameter (= 0.2 mm) was smaller than the wavelength in the liver tissue (~ 1.2 mm). The thermocouple needle was inserted about 1.6 mm along 40 degrees on the surface by using a 3D motion stage to reach the tissue depth of about 1 mm from the surface (Fig. 7(b)). In the same manner, the thermocouple tip was inserted at a depth of 3.0 mm for the immersion operation mode (Fig. 7(c)).

The time transition of the temperature increase was monitored for 5 min for the different pulse-repetition frequencies (PRFs). The influence of the PRF condition and the maximum temperature level were evaluated though this test. Furthermore, as illustrated in Fig. 7(c), the temperature was measured with the immersed transducer to observe the influence of the operation mode. The required sonification time for tissue ablation was estimated by using the criteria introduced in (7). Meanwhile, to observe the spatial profile of temperature, a thermo-camera (A615, FLIR Systems Inc., Wilsonville, OR) was utilized, as illustrated in Fig. 8. The thermo-camera was placed 20 cm from the tissue section while the US transducer ablated the tissue. The spatial resolution and the sampling frequency were 17 μm and 50 Hz, respectively. The video for the thermo change was acquired by using a post-processing software (ResearchIR, FLIR Systems Inc., Wilsonville, OR).

For the demonstration of tissue ablation, two different operating modes were introduced: sonification on the top surface of the liver specimen (Fig. 7(b)) and inside the tissue (Fig. 7(c)). For the first operation mode, the US transducer was placed about 0.5 mm from the tissue surface by using a 3D motion stage. For the second operation mode, a small pit was made on the tissue by using a 20G size syringe needle and was sliced with a sharp knife to make an X-shaped cut. After which, the US transducer was inserted at a depth of about 2 mm from the tissue surface. The volume of the lesion for each operating mode was investigated respectively after sonification of 5 min.

III. Results

A. Transducer Characterization

Fig. 9 presents the electric responses obtained from the simulation and the experiment. In the simulation, lateral and extensional resonance modes were 0.73 and 1.33 MHz, respectively (Fig. 9(a)), and vibrational shapes were expressed as shown in Fig. 9(b). Impedance levels were 87.6 and 528.9 Ohm for each mode and impedance response. The simulation results were comparable with the impedance response (i.e., solid line in Fig. 9(a)) of the fabricated transducer. The resonance frequencies in the actual device were 0.75 and 1.28 MHz for the lateral and the extensional resonances, where impedance levels were 191.7 and 627.3 Ohm, respectively.

Fig. 10 presents the simulation results of the acoustic field. While the −6dB drop distance for the lateral mode excitation remained within 1.2 mm (Fig. 10(a)), it reached to 3.7 mm for the extensional mode (Fig. 10(b)). The higher operating frequency (1.3 MHz) exerted the vibration of tissue molecules more frequently within a unit time compared to the sub-megahertz excitation (0.73 MHz); hence, we adopted 1.3 MHz for the operation frequency. Fig. 10(c) compares the acoustic intensity levels of the transducers with the single (i.e., 1 mm thickness) and the double (i.e., 500 μm thickness for each) layers, respectively. Under the same voltage input, the acoustic intensity (spatial-peak temporal averaged; SPTA) of the double layer transducer was about 2.5-folds greater than the single layer transducer.

The acoustic pressure output induced by the transducer was about 4.63 MPa (peak-to-peak) at a distance of 1.5 mm from the aperture under 250 V_{pp} electric input. The simulated pressure output was comparable to the result of the hydrophone test, as shown in Fig. 11(a). The acoustic pressure output upon 250 V_{pp} actuation was about 4.72 MPa in the peak-to-peak level and 2.23 MPa in the peak-negative level. This pressure level corresponded to the acoustic intensity of 185.6 W/cm^2 for the continuous signal input. For the pulse input, the acoustic intensity was predicted in Fig. 11(b). Upon the application of 250 V_{pp} with 20 % duty cycle, the acoustic intensity reached 37.6 W/cm^2, and the required electric power was estimated to be about 16.7 W. Table III tabulates the performance of the developed transducer.

Finally, temperature elevation upon insonation was predicted using the Green function-based solution introduced in (3). The prediction of the temperature elevation was made within the −6dB drop distance. Fig. 12 shows the temperature transitions over time with different acoustic power intensities. The higher the value of the acoustic intensity was, the higher and faster the temperature became. This result indicates that the acoustic intensity of about 20 W/cm^2 is required to achieve a temperature rise of 43°C within 5 min. This theoretical study therefore exhibited that the voltage magnitude of 250 V_{pp} and the duty cycle of 20% is sufficient to induce hyperthermia in liver tissue. Although this analytical approach had some errors when compared to the actual test results, which was due to the lack of PRF influence in the model, it provided a relevant guideline for the operation of the device.

B. Ex Vivo Test Results

The performance of various aspects of the developed transducer was assessed though ex vivo tests. First, the steady state temperature upon insonation was evaluated with different PRF conditions (Fig. 13). This test was necessary since the theoretical and simulation results did not fully account for the hyperthermia effect with the PRF. Under the PRF condition of 400 Hz, the temperature was raised marginally (< 4°C). To achieve a sufficient degree of temperature, the lower PRF cases were studied from 200 to 67 Hz PRF. At a PRF of 67 Hz, tissue temperature elevated up to 49.2°C, which was enough to induce the hyperthermia effect in the tissue, such that the lower PRF case (e.g., < 50 Hz) was attempted no further. Under the 67 Hz PRF condition with the surface mode, temperature stabilized within 1 min and was sustained for 5 min without a significant drop (< 0.5°C). From the temperature transition curve and the criteria in (7), the required treatment time for coagulative necrosis

was estimated to be 4 min. For the immersion mode, the temperature further elevated up to 51.9°C.

The temperature profile during insonation was captured through the thermo-camera. Fig. 14(a) presents the thermal image captured after insonation of 2 min. Meanwhile, Fig. 14(b) presents the temperature profile extracted along the axial direction of the transducer. The maximum temperature of 45.2°C was observed at about 1 mm distance from the transducer aperture. Temperature increase over 43°C was detected in the spatial span of about 3 mm. Notably, the temperature profile was well sustained during the treatment of 5 min.

Fig. 15 and 16 show liver tissues exposed to the ultrasonic beam for 5 min. For the surface sonification (Fig. 7(b)), the discolored portion was clearly observed, as shown in Fig. 15. After leaving the specimen in the atmosphere for 20 min, the irreversible change was confirmed. The section view exhibited that the tissue was ablated in the range of up to 1.0 mm from the surface. The lesion volume in the HIFU treatment was about 2.5 × 2.5 × 1.0 mm^3. For the immersing sonification (Fig. 7(c)), the tissue ablation was realized inside the pit of the tissue as well (Fig. 16). While the volume of the lesion was almost similar to the surface sonification, the side walls in the pit were additionally ablated within the range of about 0.5 mm.

IV. Discussions

The characteristics of the developed transducer were first investigated through simulation and experimental results. In this study, the resonance frequency of the extensional mode was used for the operation of the transducer because the acoustic beam reached farther distance compared to the lateral mode case as simulated in Fig. 10. The electric response in the actual transducer demonstrated reliable agreement with that of the simulated model, with 3.9% error in the resonance frequency and 18.6% in the impedance level (Fig. 9). The error in the impedance level might be caused by the additional volume and mass of backing material in the actual transducer, which was not included in the simplified boundary condition for the air backing. Based on the frequency response and the acoustic simulation results, the operating frequency of 1.3 MHz was chosen. While the miniaturized multilayered transducer reported by [26] operates in the sub-megahertz range (< 0.65 MHz), the operation frequency of the transducer presented in this study more effectively extend the near-field zone than [29]. To further increase the resonance frequencies, as presented in some other interstitial transducers (3–10 MHz) [27,28,30], thinner active layers could be utilized although these require greater electric input to obtain similar acoustic intensity due to the reduced capacitance of active layers. Furthermore, US waves with high frequency terms are more readily attenuated during the propagation inside a bio tissue [51]. The developed transducer achieved the acoustic intensity of over 37 W/cm^2 (Table III), which delivered sufficient acoustic intensity (>10 W/cm^2) to induce the coagulation necrosis of the tissue [52].

Through ex vivo test results, temperature elevation and tissue ablation were successfully demonstrated (Fig. 13). First, temperature in the experimental result rose much quicker than the analytical prediction (e.g., the 95% rise time for the case of 67 Hz PRF was faster by over 75% compared to the theoretic model). Heat dissipation during sonification could be a

possible cause although the contribution might be marginal. Accordingly, the inertial cavitation effect, which was not addressed in the analytical model, could be a potential reason for the prediction error. Past studies in [53][54] exhibited that a relatively strong rarefactional pressure can cause tissue destruction through the cavitation effect. For example, based on the transducer characterization result in Fig. 11(a), the US transducer is capable of generating rarefactional acoustic pressure over 2.2 MPa. The mechanical index corresponds to the value of 1.9, which is sufficient to cause the inertial cavitation of the tissue. The cavitation effect can therefore result in additional hyperthermia effect during sonification. Second, the equivalent thermal dose (EM_{43} ~ 273 min) was greater by 13.8% for the surface operation condition than the threshold of 240 min. This result indicated that a sufficient degree of the thermal dose was applied to the tissue, causing thermal necrosis. The estimation also showed that in this device, a minimum of 4 min is needed to achieve the equivalent thermal dose (EM_{43}) of 240 min. The therapeutic time within 5 min is relatively quick compared to other typical noninvasive HIFUs [55][56]. Third, the degree of the hyperthermia effect was controllable by adjusting the PRF condition in a fixed duty cycle. A low PRF was preferred to heat up the tissue more quickly to reach the maximum temperature range, as shown in Fig. 13. This observation indicates that the persistent vibration of the tissue molecule helps to more efficiently generate heat energy inside the tissue, reducing the thermal relaxation rate. Fourth, the temperature profile (Fig. 14) demonstrated that the inner portion of the tissue also experienced the hyperthermia effect within the spatial range of about 3 mm upon sonification. The maximum temperature in the thermo-camera test was lower than the needle-type thermocouple by about 4°C (see Fig. 13 and 14(b)). For the thermo-camera test, the tissue section was directly exposed to the water medium; heat energy was thus more likely to be dissipated to the surrounding water media. In contrast, in the needle-type thermocouple test, the thermocouple was embedded in the tissue and was not directly exposed; thus, thermal energy was better captured inside the tissue, minimizing energy dissipation. Finally, the irreversible tissue damage was investigated after 5 min of treatment, as shown in Fig. 15 and 16. This result demonstrated how the intracavitary transducer can reduce the US treatment time by interacting directly with the tissue. An additional operation mode (i.e., inserting the device into a pit) also ablated the inner part of the body organ with the volume of the lesion the same as that of the surface insonation case. Tissue along the side walls of the transducer was affected by the lateral vibration of the US transducer; nonetheless, the side ablation did not spread widely over the range of 0.5 mm (Fig. 16). In the immersion mode (Fig. 7(c)), tissue temperature was elevated more (i.e., as much as 5.5%) than the surface mode, as shown in Fig. 13. This further increase in temperature could be caused by either the lateral wave motion or the heat of the transducer. Accordingly, heat energy captured inside the tissue could be less dissipated to the water than the surface mode. The immersion operation mode demonstrated in this study can provide an additional therapeutic option; for example, the US device can approach a target with minimal incision and destruct a part of the tissue without vast surgery or tissue extraction in the similar manner shown in [57].

The current design can still be enhanced. For example, the −6dB distance needs to be extended over 10 mm to broaden the usable spatial range inside the body, minimizing the surgical area. Moreover, the lesion volume of the current device remains in the mm^3 range,

which is much smaller than that of existing US transducers in cm^3 range [58][59]. Due to the limitation of the small aperture design, it is difficult to extend the therapeutic range along the lateral direction; nevertheless, the lesion along the axial direction could be elongated in 'cm' unit by improving the current design of the transducer. In an actual bio tissue, the influence of blood perfusion is not negligible; it may degrade the efficacy of the hypothermia effect. The US device should thus be operated either in a lower PRF or with a higher electric input power to make up the perfusion effect. Similarly, adding more active layers can be considered since the axial dimension of the intracavitary transducer is less restricted compared to the lateral dimension. By adding more active layers, acoustic intensity under the same electric input (e.g., 250 V_{pp}) could be further increased. The multilayer transducer should be consequently designed by comprehensively considering change in resonance frequency. Moreover, composite-type of active layers can be considered to extend the therapeutic range; the predominant extensional motion of the composite can transmit acoustic power to a relatively farther distance.

Despite the limitations of the current technology, this study demonstrated that the miniaturized, forward-looking transducer was capable of inducing irreversible tissue damage within 5 min and with a relatively small electric power input of 16.7 W. Furthermore, the ex vivo test results were promising as they showed the potential medical application of precise tissue ablation, significantly reducing the risk of unintended tissue damage.

V. Conclusions

This article proposed a miniaturized intracavitary forward-looking US transducer that can be inserted through an endoscopic device, such as bronchoscope, for deep-organ tumor ablation. The developed device was capable of generating the acoustic intensity of 37.1 W/cm^2 from the small aperture, with a relatively low electric power (< 17 W). The analytical bio-heat model and the simulation results demonstrated that acoustic intensity was sufficient for tissue ablation. The performance of the developed transducer was validated through *ex vivo* test results using porcine livers. The temperature inside the tissue was elevated up to 49.2°C and 51.8°C for the surface and the immersion operation modes, respectively. Furthermore, therapeutic efficacy was demonstrated by insonating the tissue for 5 min. The lesion volume was about $2.5 \times 2.5 \times 1.0$ mm^3, which resulted in irreversible tissue damage in the insonated tissue volume. The prototyped transducer provides a promising therapeutic option that is capable of directly ablating tissue inside the body using an endoscopic device, such as a bronchoscope. Although the therapeutic efficacy of the intracavitary US transducer was successfully demonstrated in this study, further improvement can be made to enhance acoustic intensity and to extend the therapeutic range.

Acknowledgements

This work was supported in part by the National Institutes of Health under grant R01HL141967 and Duke Incubation Fund. The authors would like to thank Dr. Yong Zhu for the technical support on the thermo-camera.

References

[1]. Kennedy JE, “High-Intensity Focused Ultrasound in the Treatment of Solid Tumours,” Nature Reviews Cancer, Vol. 5, No. 4, pp. 321–327, 2005. [PubMed: 15776004]

[2]. Chaussy CG and Thüroff S, “High-Intensity Focused Ultrasound for the Treatment of Prostate Cancer: a Review,” Journal of Endourology, Vol. 31, No. S1, pp. S30–37, 2017. [PubMed: 28355119]

[3]. Wu F, Wang ZB, Cao Y-D, Zhu X-Q, Zhu H, Chen WZ, and Zou JZ, “Wide Local Ablation of Localized Breast Cancer Using High Intensity Focused Ultrasound,” Journal of Surgical Oncology, Vol. 96, No. 2, pp. 130–136, 2007. [PubMed: 17443737]

[4]. Al-Bataineh O, Jenne J, and Huber P, “Clinical and Future Applications of High Intensity Focused Ultrasound in Cancer,” Cancer Treatment Reviews, Vol. 38, No. 5, pp. 346–353, 2012. [PubMed: 21924838]

[5]. Brace C, “Thermal Tumor Ablation in Clinical Use,” IEEE Pulse, Vol. 2, No. 5, pp. 28–38, 2011.

[6]. Ter Haar G, “Therapeutic Applications of Ultrasound,” Progress in Biophysics and Molecular Biology, Vol. 93, No. 1–3, pp. 111–129, 2007. [PubMed: 16930682]

[7]. Diederich CJ, Stafford RJ, Nau WH, Burdette EC, Price RE, and Hazle JD, “Transurethral Ultrasound Applicators with Directional Heating Patterns for Prostate Thermal Therapy: In Vivo Evaluation Using Magnetic Resonance Thermometry,” Medical Physics, Vol. 31, No. 2, pp. 405–413, 2004. [PubMed: 15000627]

[8]. Damianou C, “In Vitro and In Vivo Ablation of Porcine Renal Tissues Using High-Intensity Focused Ultrasound,” Ultrasound in Medicine & Biology, Vol. 29, No. 9, pp. 1321–1330l, 2003. [PubMed: 14553810]

[9]. Guo S, Jing Y, and Jiang X, “Temperature Rise in Tissue Ablation Using Multi-Frequency Ultrasound,” IEEE Transactions on Ultrasonics, Ferroelectrics, and Frequency Control, Vol. 6, No. 8, pp. 1699–1707, 2013.

[10]. Klingler HC, Susani M, Seip R, Mauermann J, Sanghvi N, Marberger MJ, “A Novel Approach to Energy Ablative Therapy of Small Renal Tumours: Laparoscopic High-Intensity Focused Ultrasound,” European Urology, Vol. 53, No. (4), pp. 810–818, 2008. [PubMed: 18069120]

[11]. Zhang X, Macoskey JJ, Ives K, Owens GE, Gurm HS, Shi J, and Xu Z, “Non-Invasive Thrombolysis Using Microtripsy in a Porcine Deep Vein Thrombosis Model,” Ultrasound in Medicine & Biology, Vol. 43, No. 7, 1378–1390, 2017. [PubMed: 28457630]

[12]. Ramaekers P, De Greef M, Van Breugel JMM, Moonen CTW, and Ries M, “Increasing the HIFU Ablation Rate through an MRI-Guided Sonication Strategy Using Shock Waves: Feasibility in the In Vivo Porcine Liver,” Physics in Medicine & Biology, Vol. 61, No. 3, pp. 10571077, 2016.

[13]. O’rourke AP, Haemmerich D, Prakash P, Converse MC, Mahvi DM, and Webster JG, “Current Status of Liver Tumor Ablation Devices,” Expert Review of Medical Devices, Vol. 4, No. 4, pp. 523–537, 2007. [PubMed: 17605688]

[14]. Goldberg SN, Ahmed M, Gazelle GS, Kruskal JB, Huertas JC, Halpern EF, Oliver BS, Lenkinski RE, “Radio-Frequency Thermal Ablation with NaCl Solution Injection: Effect of Electrical Conductivity on Tissue Heating and Coagulation - Phantom and Porcine Liver Study,” Radiology, Vol. 219, No. 1, pp. 157–165, 2001. [PubMed: 11274551]

[15]. Mahmood K and Wahidi MM, “Ablative Therapies for Central Airway Obstruction,” Seminars in Respiratory and Critical Care Medicine, Vol. 35, No. 6, pp. 681–692, 2014. [PubMed: 25463159]

[16]. Lubner MG, Brace CL, Hinshaw JL, and Lee FT Jr, “Microwave Tumor Ablation: Mechanism of Action, Clinical Results, and Devices,” Journal of Vascular and Interventional Radiology, Vol. 21, No. 8, pp. S192–S203, 2011.

[17]. Simon CJ, Dupuy DE, and Mayo-Smith WW, “Microwave Ablation: Principles and Applications,” Radiographics, Vol. 25, pp. S69–S83, 2005. [PubMed: 16227498]

[18]. Miyazaki S, Nakamura H, Taniguchi H, Hachiya H, Takagi T, Igarashi M, Kajiyama T, Watanabe T, Niida T, Hirao K, and Iesaka Y, “Gastric Hypomotility after Second-Generation Cryoballoon Ablation - Unrecognized Silent Nerve Injury after Cryoballoon Ablation,” Heart Rhythm, Vol. 14, No. 5, pp. 670–677, 2017. [PubMed: 28434448]

[19]. Kuck KH, Brugada J, Fürnkranz A, Metzner A, Ouyang F, Chun KJ, and Albenque JP, "Cryoballoon or Radiofrequency Ablation for Paroxysmal Atrial Fibrillation," New England Journal of Medicine, Vol. 374, No. 23, pp. 2235–2245, 2016. [PubMed: 27042964]

[20]. Mozo M, Gonzálo R, Gutiérrez JM, Gutiérrez LE, Cotruta L, Roca A, and García R, "Colorenal Fistula after Renal Tumour Cryotherapy," International Journal of Surgery Case Reports, Vol. 53, pp. 441–443, 2018. [PubMed: 30567064]

[21]. Illing RO, Kennedy JE, Wu F, Ter Haar GR, Protheroe AS, Friend PJ, and Middleton MR, "The Safety and Feasibility of Extracorpoeal High-Intensity Focused Ultrasound (HIFU) for the Treatment of Liver and Kidney Tumours in a Western Population," British Journal of Cancer, Vol. 93, No. 8, pp. 890–895, 2005. [PubMed: 16189519]

[22]. Wang M, Yuan W, Jiang X, Jing, Y Y, and Wang Z, "Disruption of Microalgal Cells Using High-Frequency Focused Ultrasound," Bioresource Technology, Vol. 153, pp. 315–321, 2014. [PubMed: 24374364]

[23]. Owens CA, "Ultrasound-Enhanced Thrombolysis: EKOS EndoWave Infusion Catheter System." Seminars in Interventional Radiology, Vol. 25 No. 1, pp. 37–41, 2008. [PubMed: 21326491]

[24]. Liu X, Ellens N, Williams E, Burdette EC, Karmarkar P, and Bottomley P, "A Combined Intravascular MRI Endoscope and Intravascular Ultrasound (IVUS) Transducer for High-Resolution Image-Guided Ablation," Proceedings of the International Society for Magnetic Resonance in Medicine Scientific Meeting and Exhibition, Vol. 25, 2017.

[25]. Jiang X and Al-Jumaily AM, "Ultrasound Transducers for Biomedical Imaging and Therapy," Journal of Engineering and Science in Medical Diagnostics and Therapy, Vol. 1, No. 4, 040201, 2018.

[26]. Kim J, Lindsey BD, Chang WY, Dai X, Stavas JM, Dayton PA, and Jiang X, "Intravascular Forward-Looking Ultrasound Transducers for Microbubble-Mediated Sonothrombolysis," Scientific Reports, Vol. 7, No. 3454, 2017.

[27]. Chopra R, Baker N, Choy V, Boyes A, Tang K, Bradwell D, and Bronskill MJ, "MRI-Compatible Transurethral Ultrasound System for the Treatment of Localized Prostate Cancer Using Rotational Control," Medical Physics, Vol. 35, No. 4, pp. 1346–1357, 2008. [PubMed: 18491529]

[28]. Ross AB, Diederich CJ, Nau WH, Gill H, Bouley DM, Daniel B, Rieke V, Butts RK, and Sommer G, "Highly Directional Transurethral Ultrasound Applicators with Rotational Control for MRI-Guided Prostatic Thermal Therapy," Physics in Medicine & Biology, Vol. 49, No. 2, pp. 189–204, 2004. [PubMed: 15083666]

[29]. Canney MS, Chavrier F, Tsysar S, Chapelon JY, Lafon C, and Carpentier A, "A Multi-Element Interstitial Ultrasound Applicator for the Thermal Therapy of Brain Tumors," The Journal of the Acoustical Society of America, Vol. 134, No. 2, pp. 1647–1655, 2013. [PubMed: 23927205]

[30]. Lafon C, Melodelima D, Salomir R, and Chapelon JY, "Interstitial Devices for Minimally Invasive Thermal Ablation by High-Intensity Ultrasound," International Journal of Hyperthermia, Vol. 23, No. 2, pp. 153–163, 2007. [PubMed: 17578339]

[31]. Sommer K. B. Pauly, Holbrook A, Plata J, Daniel B, Bouley D, Gill H, Prakash P, Salgaonkar V, Jones P, and Diederich C, "Applicators for MR-Guided Ultrasonic Ablation of BPH," Investigative Radiology, Vol. 48, No. 6, pp. 387–394, 2013. [PubMed: 23462673]

[32]. Nakagawa H, Antz M, Wong T, Schmidt B, Ernst S, Ouyang F, and Po SS, "Initial Experience Using a Forward Directed, High-Intensity Focused Ultrasound Balloon Catheter for Pulmonary Vein Antrum Isolation in Patients with Atrial Fibrillation," Journal of Cardiovascular Electrophysiology, Vol. 18, No. 2, pp. 136–144, 2007. [PubMed: 17239138]

[33]. Owen NR, Bouchoux G, Seket B, Murillo-Rincon A, Merouche S, Birer A, and Fleury G, "In Vivo Evaluation of a Mechanically Oscillating Dual-Mode Applicator for Ultrasound Imaging and Thermal Ablation," IEEE Transactions on Biomedical Engineering, Vol. 57, No. 1, pp. 80–92, 2009. [PubMed: 19497808]

[34]. Prat F, Lafon C, de Lima DM, Theilliere Y, Fritsch J, Pelletier G, Buffet C, and Cathignol D, "Endoscopic Treatment of Cholangiocarcinoma and Carcinoma of the Duodenal Papilla by Intraductal High-Intensity US: Results of a Pilot Study," Gastrointestinal Endoscopy, Vol. 56, No. 6, pp. 909–915, 2002. [PubMed: 12447312]

[35]. Makin IRS, Mast TD, Faidi W, Runk MM, Barthe PG, and Slayton MH, "Miniaturized Ultrasound Arrays for Interstitial Ablation and Imaging," Ultrasound in Medicine & Biology, Vol. 31, No. 11, pp. 1539–1550, 2005. [PubMed: 16286031]

[36]. Meininger GR, Calkins H, Lickfett L, Lopath P, Fjield T, Pacheco R, Harhen P, Rodriguez ER, Berger R, Halperin H, Solomon SB, "Initial Experience with a Novel Focused Ultrasound Ablation System for Ring Ablation Outside the Pulmonary Vein," Journal of Interventional Cardiac Electrophysiology, Vol. 8, No. 2, pp. 141–148, 2002.

[37]. Li T, Khokhlova T, Maloney E, Wang YN, D'Andrea S, Starr F, Farr N, Morrison K, Keilman G, and Hwang JH, "Endoscopic High-Intensity Focused US: Technical Aspects and Studies in an In Vivo Porcine Model (with Video)," Gastrointestinal Endoscopy, Vol. 81, No. 5, pp. 1243–1250, 2015. [PubMed: 25759124]

[38]. Jaunich M, Raje S, Kim K, Mitra K, and Guo Z, "Bio-Heat Transfer Analysis during Short Pulse Laser Irradiation of Tissues," International Journal of Heat and Mass Transfer, Vol. 51, No. 23–24, pp. 5511–5521, 2008.

[39]. Pennes HH, "Analysis of Tissue and Arterial Blood Temperatures in the Resting Human Forearm," Journal of Applied Physiology, Vol. 1, No. 2, pp. 93–122, 1948. [PubMed: 18887578]

[40]. Nyborg WL, "Solutions of the Bio-Heat Transfer Equation," Physics in Medicine & Biology, Vol. 33, No. 7, pp. 785, 1988. [PubMed: 3212041]

[41]. Bakker JF, Paulides MM, Obdeijn IM, Van Rhoon GC, and Van Dongen KWA, "An Ultrasound Cylindrical Phased Array for Deep Heating in the Breast: Theoretical Design Using Heterogeneous Models," Physics in Medicine & Biology, Vol. 54, No. 10, pp. 3201–3215, 2009. [PubMed: 19420416]

[42]. Elwassif MM, Kong Q, Vazquez M, and Bikson M, "Bio-Heat Transfer Model of Deep Brain Stimulation-Induced Temperature Changes," Journal of Neural Engineering, Vol. 3, No. 4, 306, 2006. [PubMed: 17124335]

[43]. Preston RC (Ed.), Output Measurements for Medical Ultrasound. Springer Science & Business Media, 2012.

[44]. Guntur SR, Lee KI, Paeng DG, Coleman AJ, and Choi MJ, "Temperature-Dependent Thermal Properties of Ex Vivo Liver Undergoing Thermal Ablation," Ultrasound in Medicine & Biology, Vol. 39, No. 10, pp. 1771–1784, 2013. [PubMed: 23932271]

[45]. Sapareto SA, and Dewey WC, "Thermal Dose Determination in Cancer Therapy," International Journal of Radiation Oncology Biology Physics, Vol 10, No. 6, pp. 787–800, 1984.

[46]. Liu Y, Kon T, Li C, and Zhong P, "High Intensity Focused Ultrasound-Induced Gene Activation in Solid Tumors," The Journal of the Acoustical Society of America, Vol. 120, No. 1, pp. 492–501, 2006. [PubMed: 16875245]

[47]. Hooker MW, Properties of PZT-Based Piezoelectric Ceramics between −150 and 250°C, NASA/CR-1998–208708, 1998.

[48]. Ma J, Guo S, Wu D, Geng X, and Jiang X, "Design, Fabrication, and Characterization of a Single-Aperture 1.5-MHz/3-MHz Dual-Frequency HIFU Transducer," IEEE Transactions on Ultrasonics, Ferroelectrics, and Frequency Control, Vol. 60, No. 7, pp. 1519–1529, 2013.

[49]. Woodacre JK, Landry TG, and Brown JA, "A Low-Cost Miniature Histotripsy Transducer for Precision Tissue Ablation," IEEE Transactions on Ultrasonics, Ferroelectrics, and Frequency Control, Vol. 65, No. 11, pp. 2131–2140, 2018.

[50]. Kim HW, Wu H, and Jiang X, "Miniaturized Sub-Megahertz Focused Ultrasound Transducer Composed of Multilayer Hard PZT Ceramics," IEEE International Ultrasonics Symposium, Kobe, Japan, 2018.

[51]. Buckingham MJ, "Theory of Acoustic Attenuation, Dispersion, and Pulse Propagation in Unconsolidated Granular Materials Including Marine Sediments," The Journal of the Acoustical Society of America, Vol. 102, No. 5, pp. 2579–2596, 1997.

[52]. Kim YS, Rhim H, Choi MJ, Lim HK, and Choi D, "High-Intensity Focused Ultrasound Therapy: An Overview for Radiologists," Korean journal of radiology, Vol. 9, No. 4, pp. 291–302, 2008. [PubMed: 18682666]

[53]. Khokhlova VA, Fowlkes JB, Roberts WW, Schade GR, Xu Z, Khokhlova TD, Hall TL, Maxwell AD, Wang YN, and Cain CA, "Histotripsy Methods in Mechanical Disintegration of Tissue:

Towards Clinical Applications," International Journal of Hyperthermia, Vol. 31, No. 2, pp. 145–162, 2015. [PubMed: 25707817]

[54]. Vlaisavljevich E, Kim Y, Owens G, Roberts W, Cain C, and Xu Z, "Effects of Tissue Mechanical Properties on Susceptibility to Histotripsy-Induced Tissue Damage," Physics in Medicine & Biology, Vol. 59, No. 2, pp. 253–270, 2013. [PubMed: 24351722]

[55]. Orsi F, Zhang L, Arnone P, Orgera G, Bonomo G, Vigna PD, Monfardini l.,, Zhou K, Chen W, Wang Z, and Veronesi U, "High-Intensity Focused Ultrasound Ablation: Effective and Safe Therapy for Solid Tumors in Difficult Locations," American Journal of Roentgenology, Vol. 195, No. 3, W245–W252, 2010. [PubMed: 20729423]

[56]. Klingler HC, Susani m., Seip R, Mauermann J, Sanghvi N, and Marberger MJ, "A Novel Approach to Energy Ablative Therapy of Small Renal Tumours: Laparoscopic High-Intensity Focused Ultrasound," European Urology, Vol. 53, No. 4, pp. 810–818, 2008. [PubMed: 18069120]

[57]. Boctor EM, Stolka P, Kang HJ, Clarke C, Rucker C, Croom J, Burdette EC, and Webster III RJ, "Precisely Shaped Acoustic Ablation of Tumors Utilizing Steerable Needle and 3D Ultrasound Image Guidance," SPIE Medical Imaging, Vol. 7625, p. 76252N, 2010.

[58]. Jung SE, Cho SH, Jang JH, and Han JY, "High-Intensity Focused Ultrasound Ablation in Hepatic and Pancreatic Cancer: Complications," Abdominal Imaging, Vol. 36, No. 2, pp. 185–195, 2011. [PubMed: 20512487]

[59]. Al-Bataineh O, Jenne J, and Huber P, "Clinical and Future Applications of High Intensity Focused Ultrasound in Cancer," Cancer Treatment Reviews, Vol. 38, No. 5, pp. 346–353, 2012. [PubMed: 21924838]

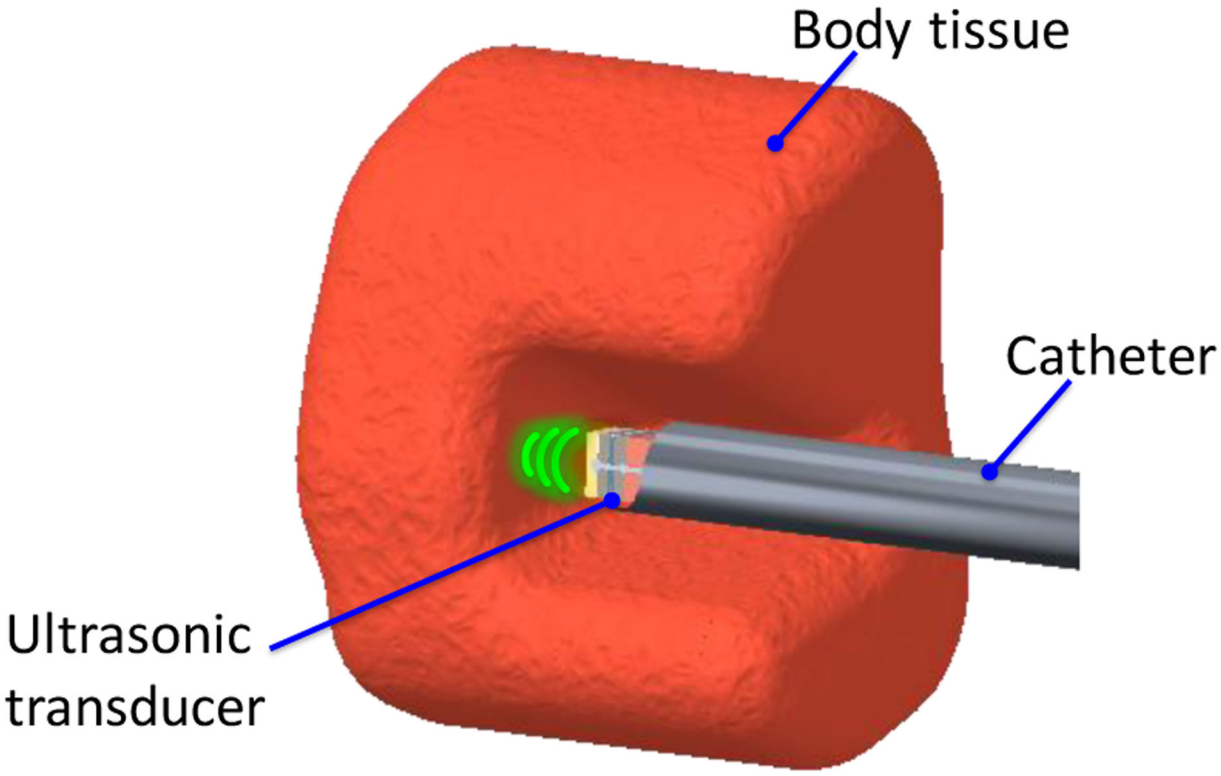

Fig. 1.
Schematic of a miniaturized intracavitary ultrasound transducer operating for ablation of body tissue.

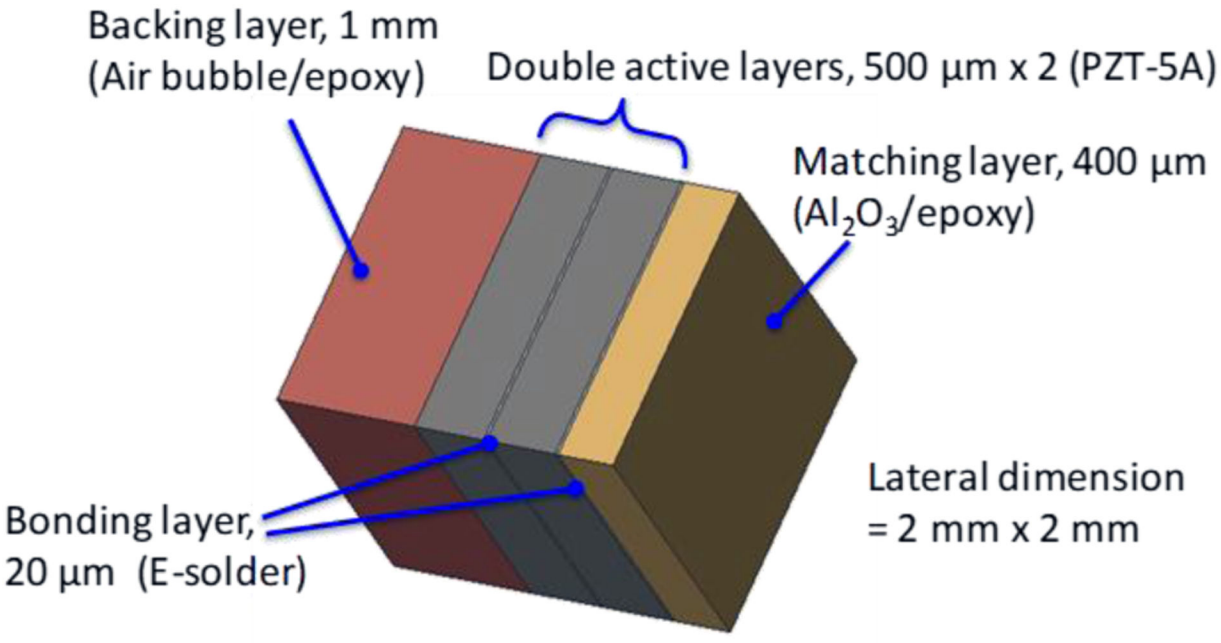

Fig. 2.
Schematic of dual-layer ultrasound transducer with the geometric and the material specifications.

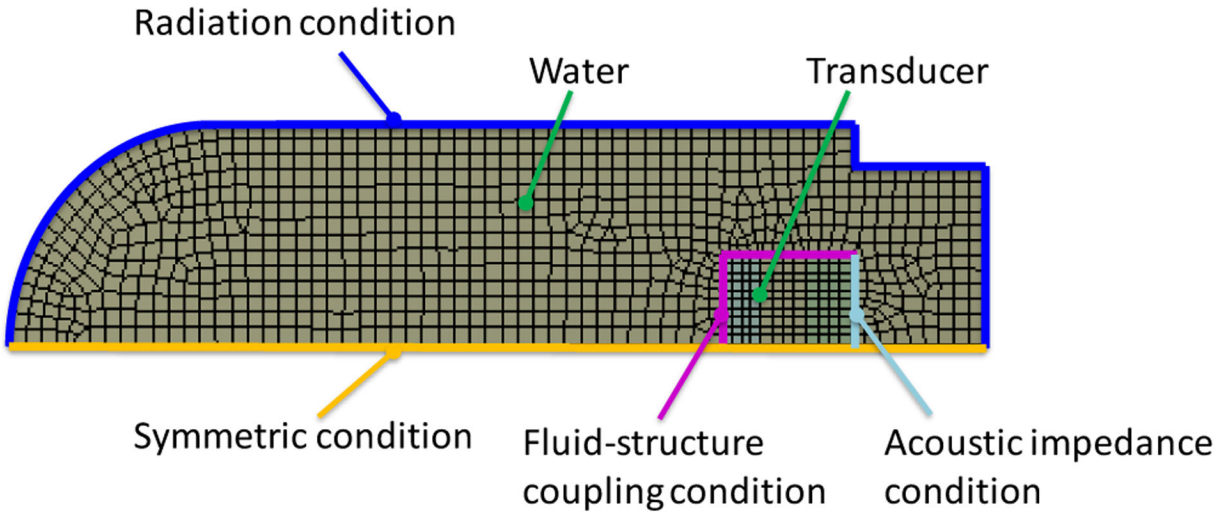

Fig. 3.
Finite element mesh and the boundary conditions for the numerical simulation.

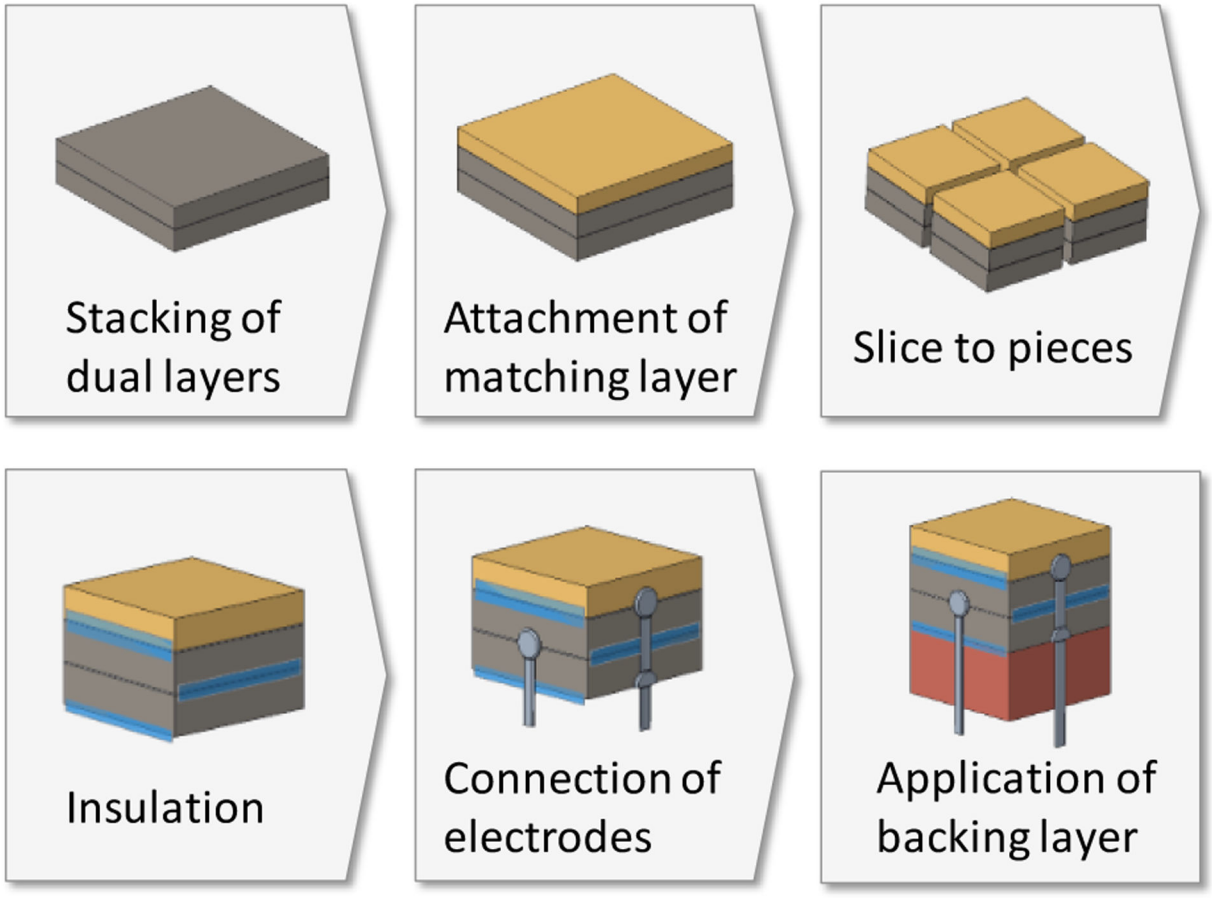

Fig. 4.
Fabrication steps for the miniaturized ultrasound transducer.

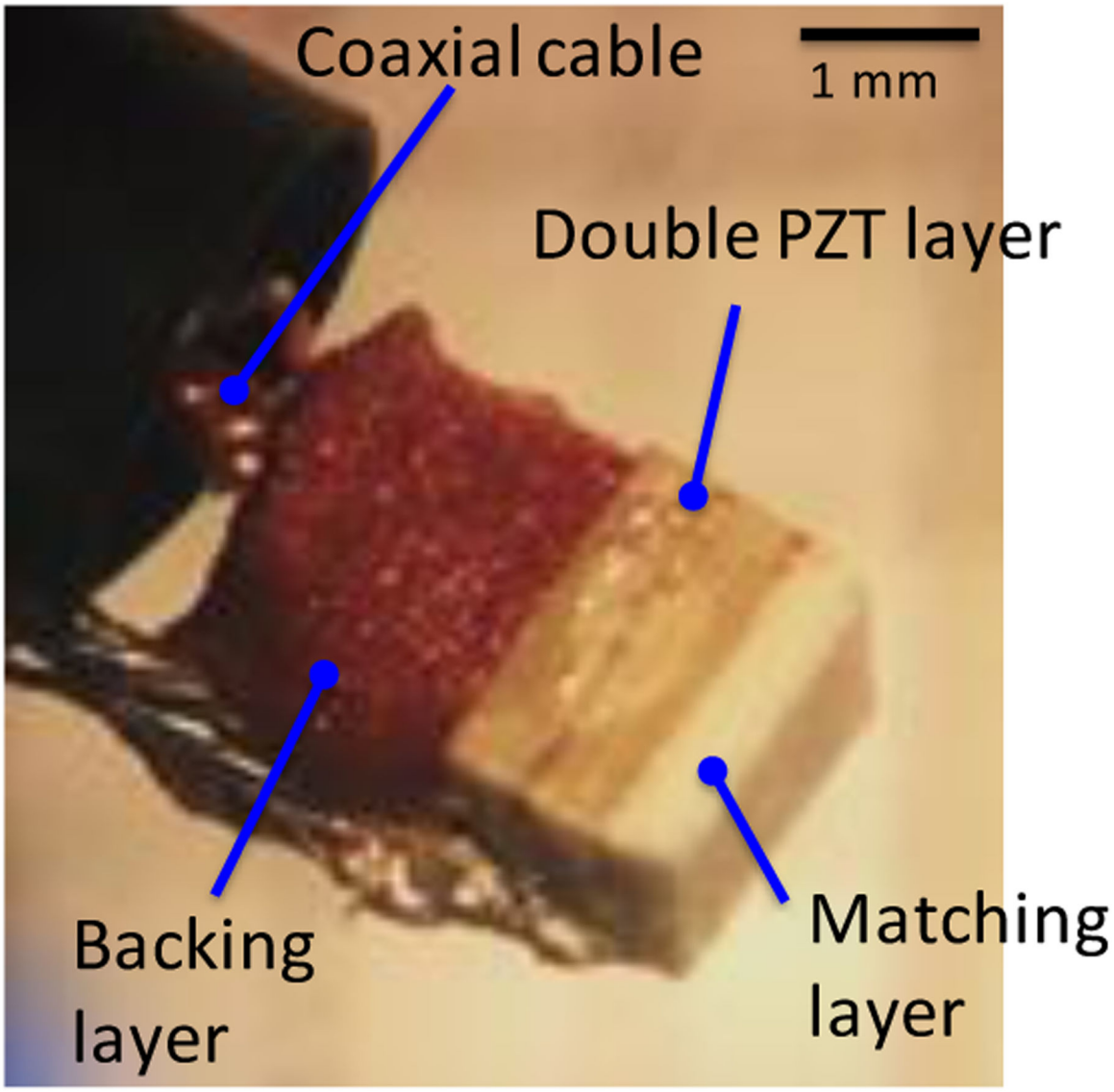

Fig. 5.
Fabricated ultrasound transducer comprised of double active elements with the matching and the backing layers.

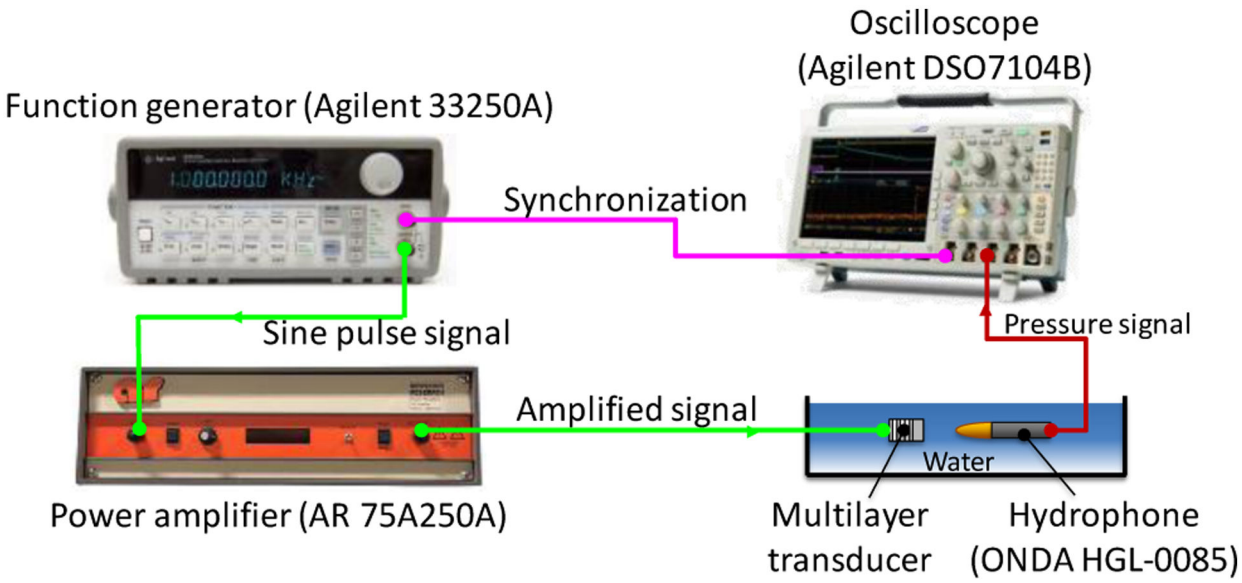

Fig. 6.

Experimental set-up for the measurement of the acoustic pressure output from the ultrasound transducer.

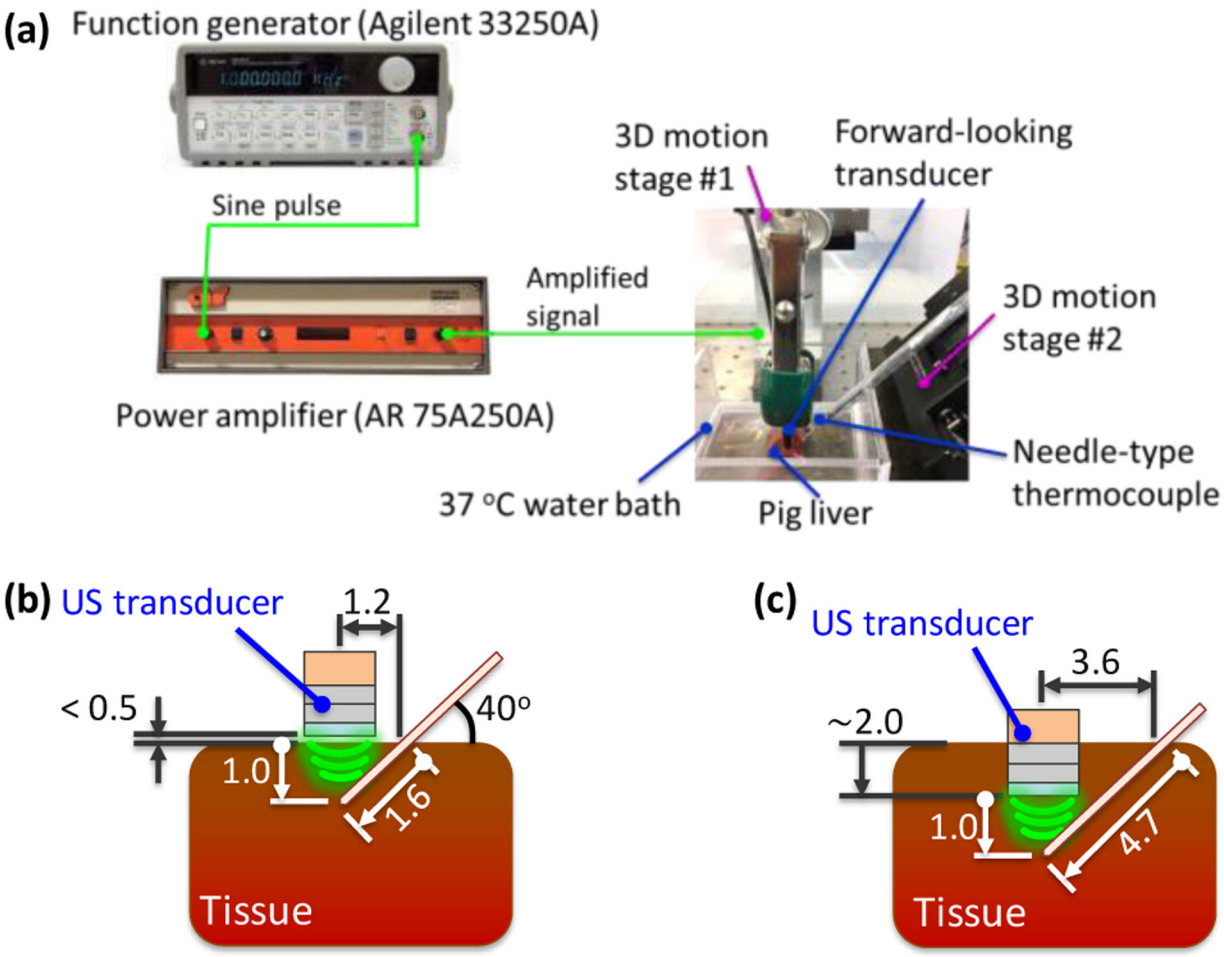

Fig. 7.

Ex vivo test for tissue ablation using the miniaturized ultrasound transducer; (a) test set-up, and (b) surface and (c) immersion operation modes.

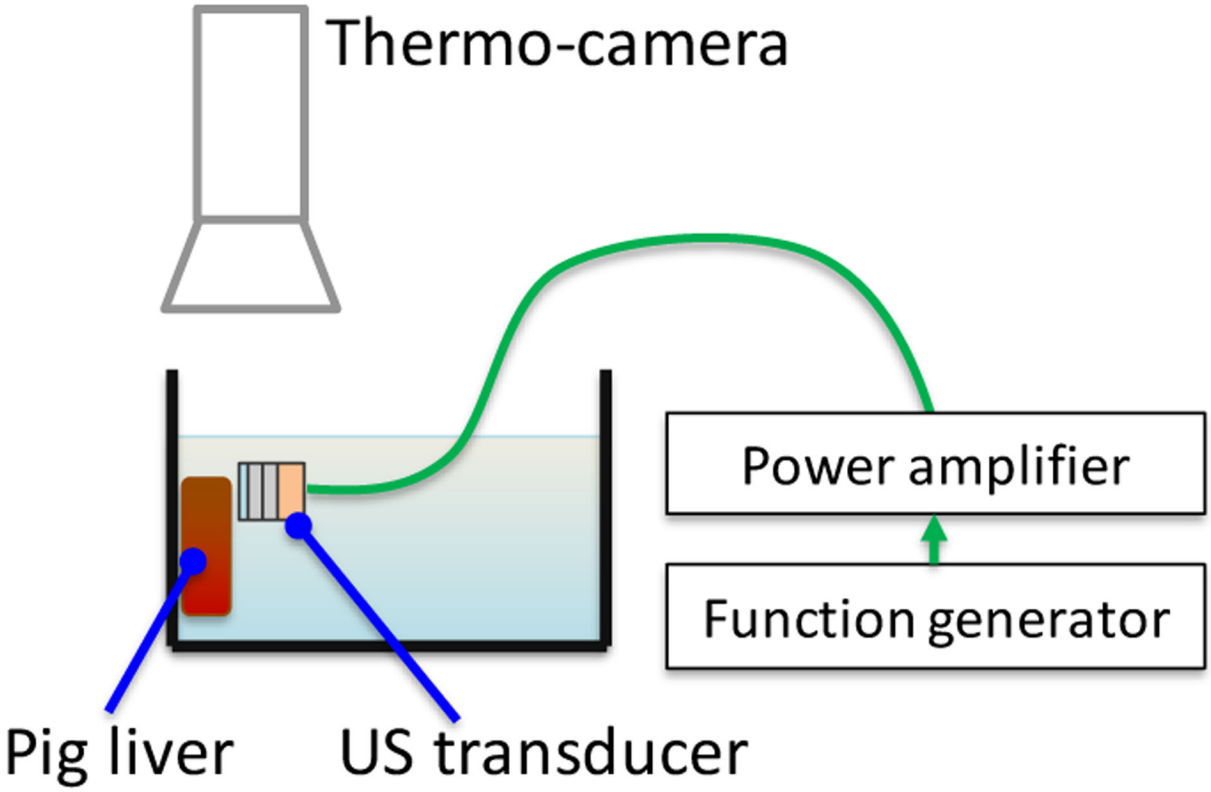

Fig. 8.
Experimental set-up to capture the spatial profile of the temperature elevation.

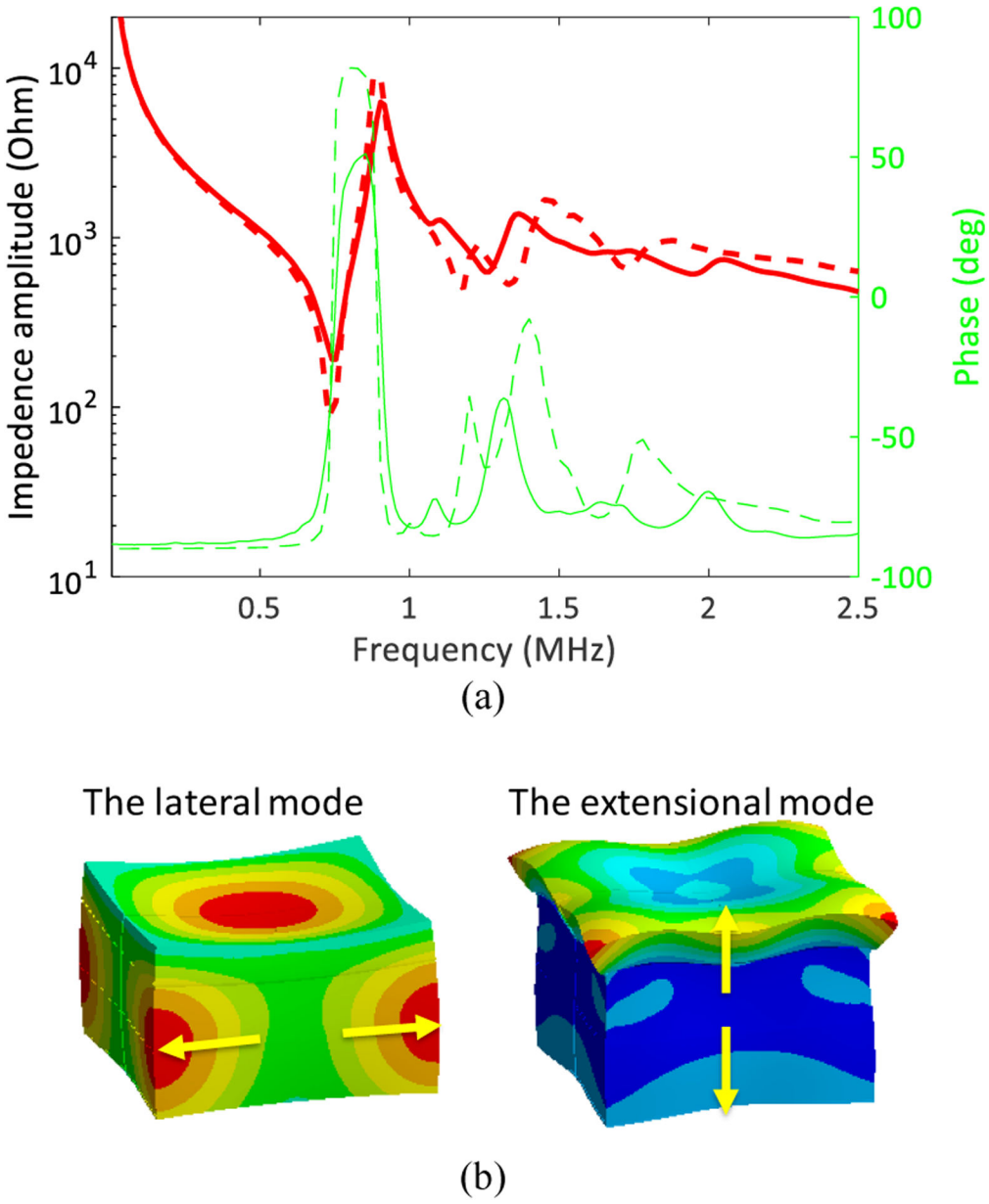

Fig. 9.

Simulation results for the transducer; (a) electric impedance curves (solid lines) comparable to the test result of the actual device and (b) the vibrational mode at the lateral and the extensional modes.

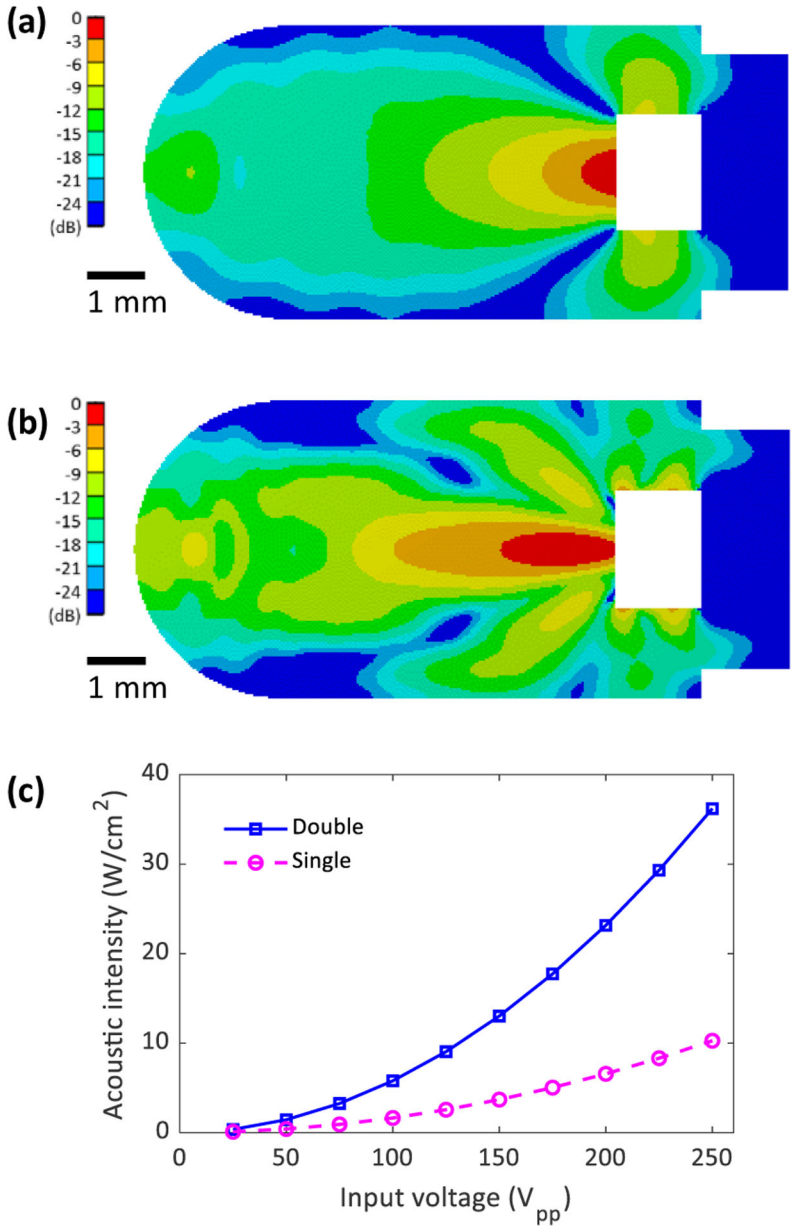

Fig. 10.

Acoustic pressure field induced by (a) the lateral mode, (b) the extensional mode of the designed transducer, and (c) the comparison of the acoustic intensity (I_{SPTA}) of the double and the single layer transducers.

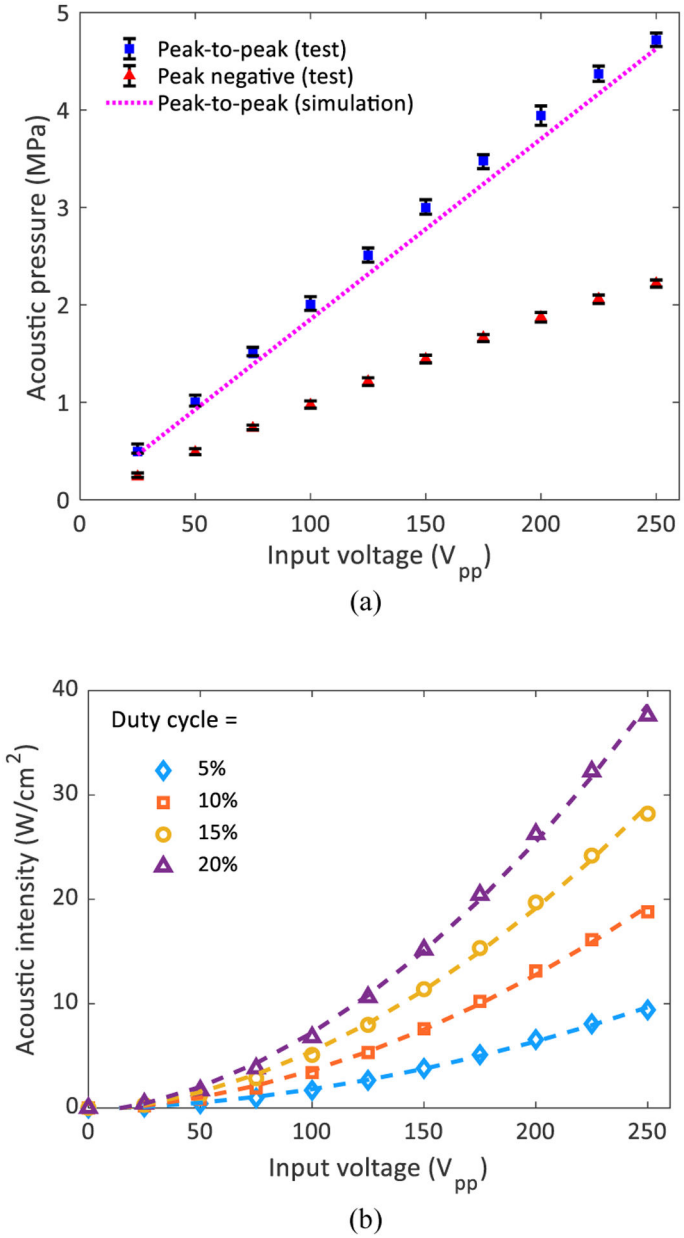

Fig. 11.

Acoustic pressure (a) induced by the transducer and the comparison with the simulation result (test number, N = 3) and the corresponding acoustic intensity (b) with respect to duty cycle.

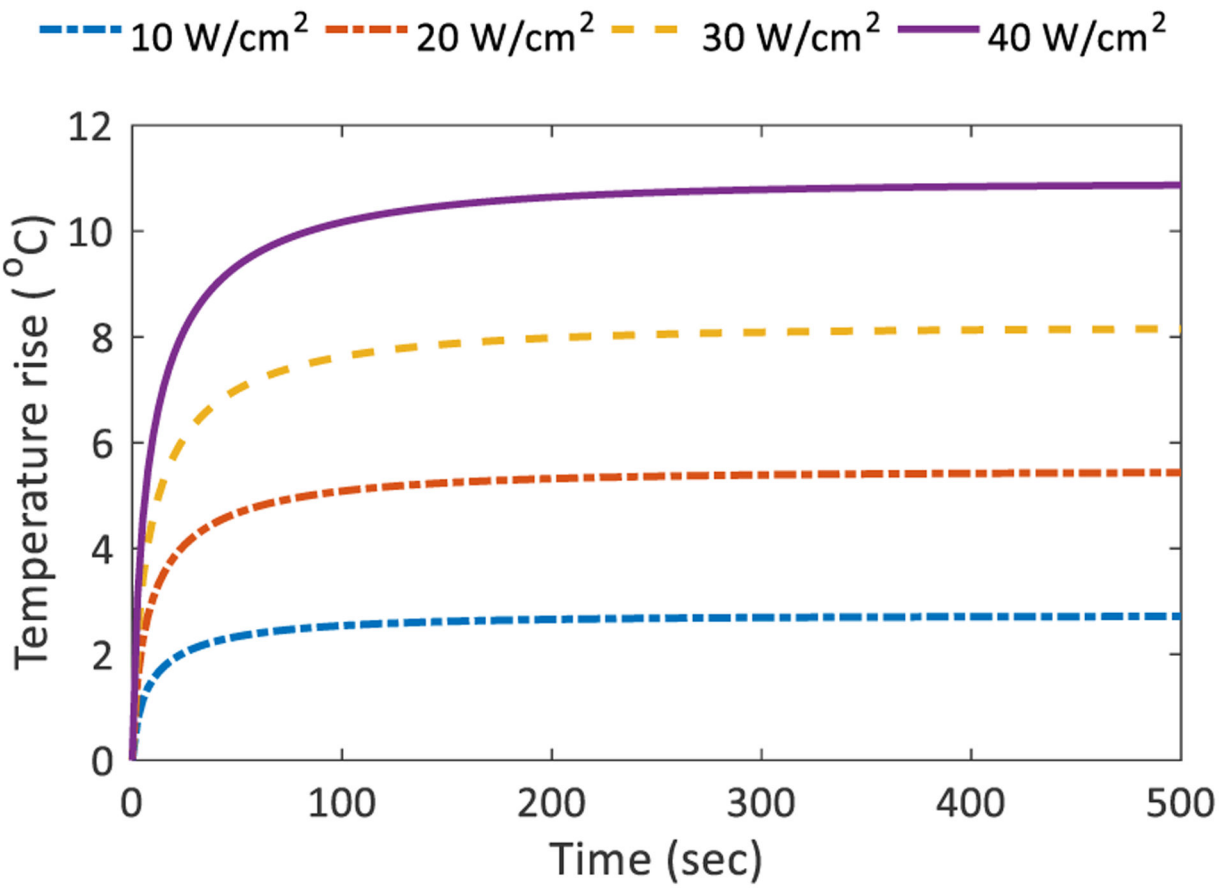

Fig. 12.
Prediction of temperature elevation over time with different acoustic power intensities, where the initial temperature is 37 °C.

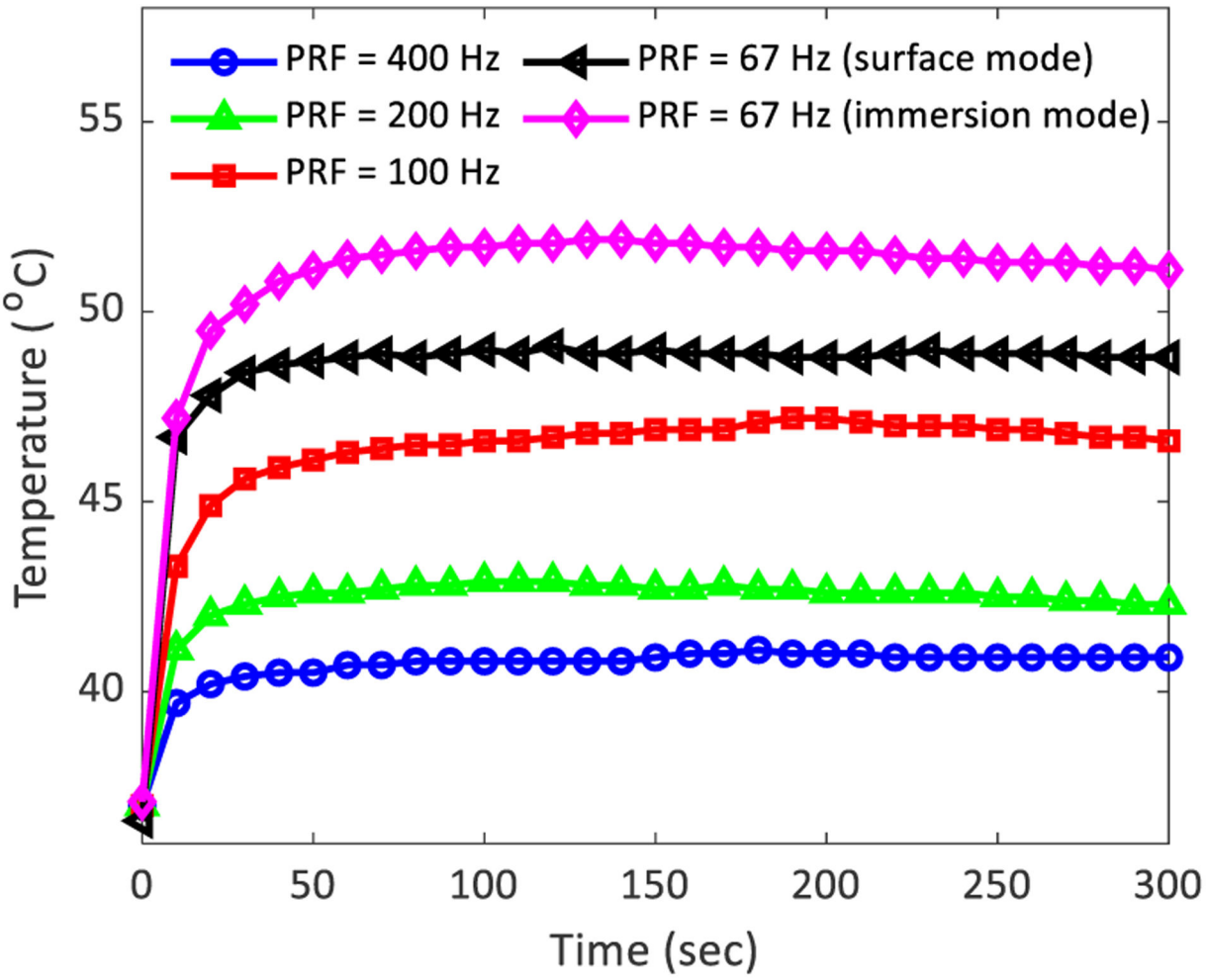

Fig. 13.
Temperature transition for five minutes with the various PRF conditions and the different operation modes (surface and immersion).

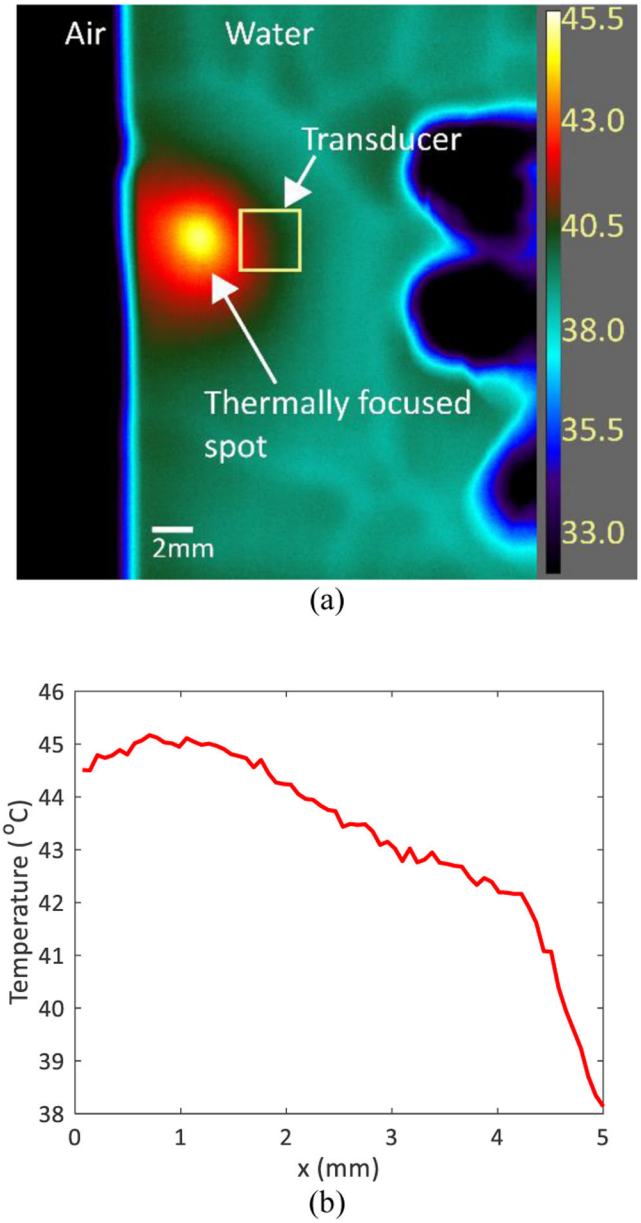

Fig. 14.

Temperature distribution of the sectional area of the tissue; (a) thermal distribution captured by thermo-camera, and (b) temperature profile from the tissue surface to the depth direction.

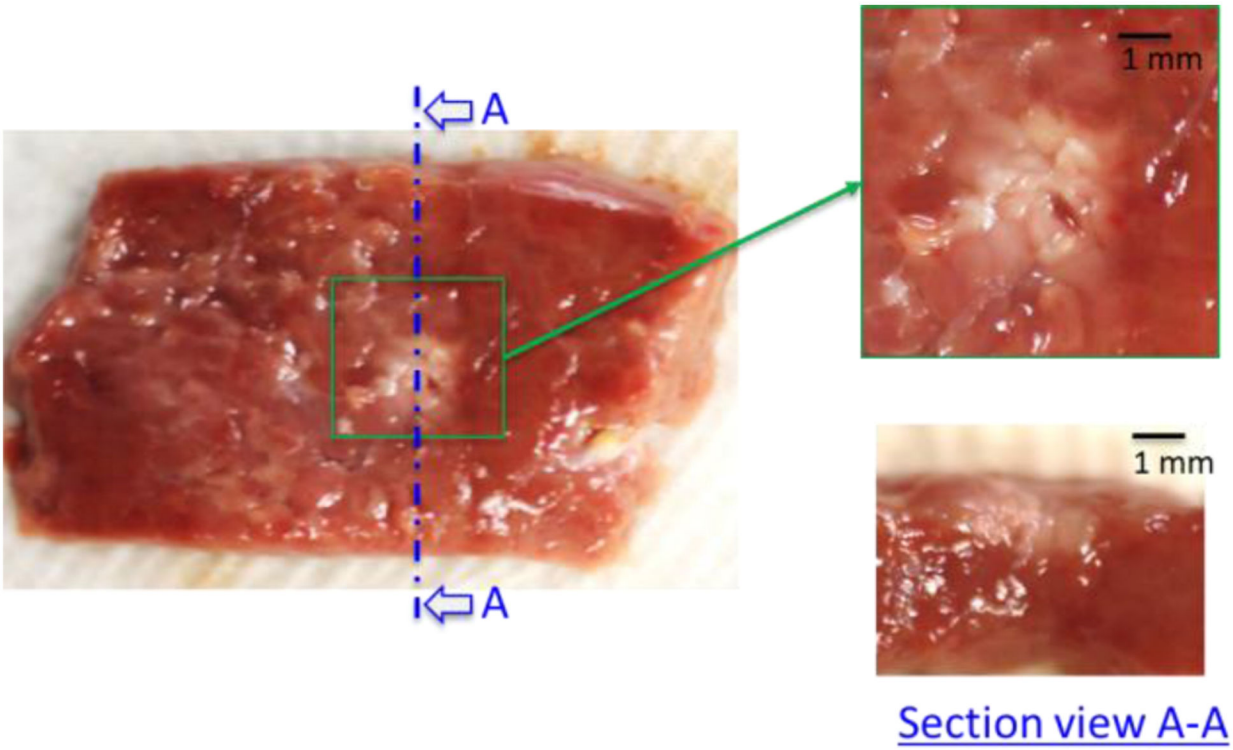

Fig. 15.

Tissue ablation by the surface sonification, where the discolored volume indicates the permanently ablated tissue.

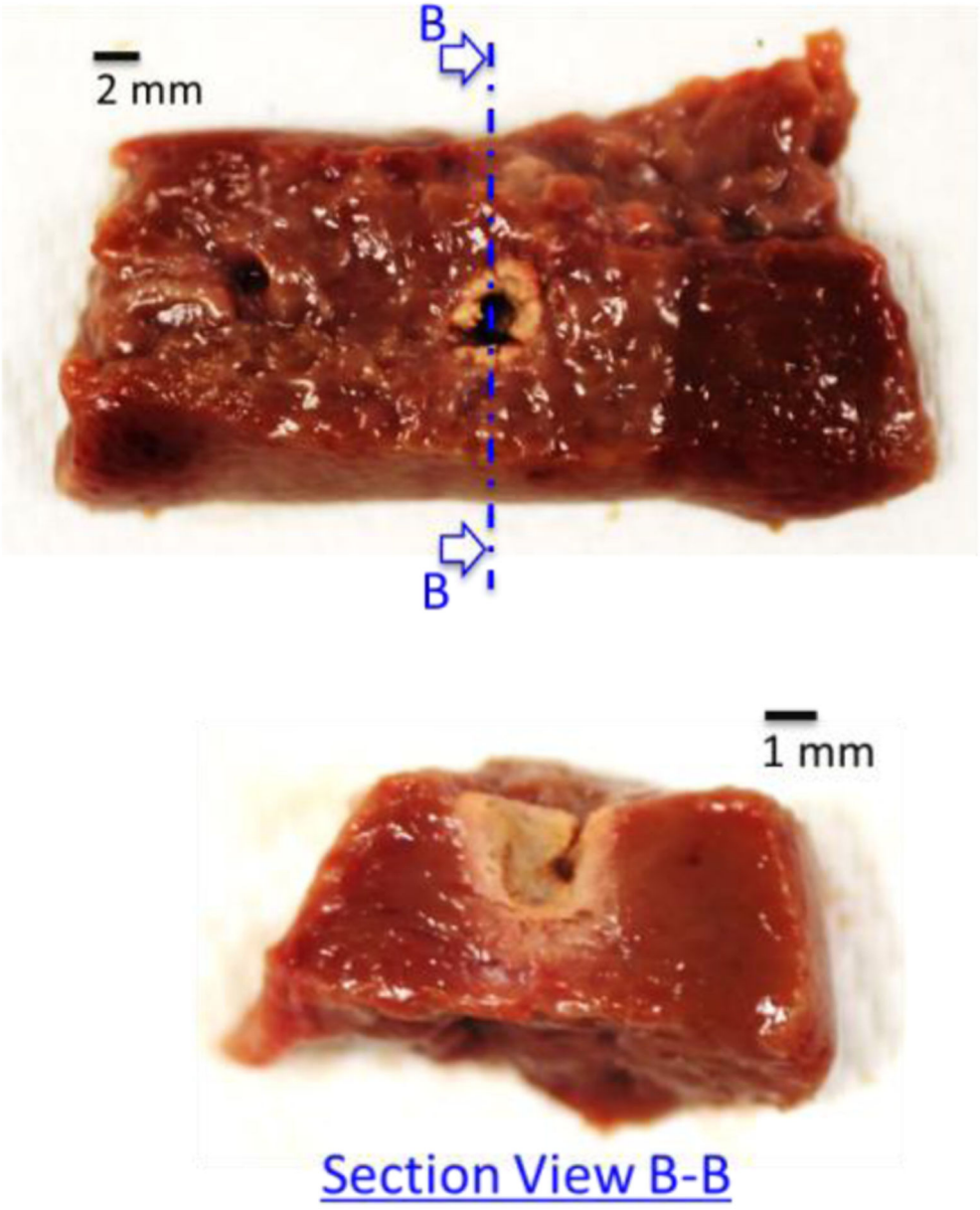

Fig. 16.
Tissue ablation by the immersing sonification, where the discolored volume indicates the permanently ablated tissue.

TABLE I

Parameters for the prediction of temperature elevation in a liver tissue [42–44].

Parameters	Symbols	Units	Values
Thermal conductivity	K	W/(m·°C)	0.52
Absorption coefficient	α	Np/m/MHz	14.0
Thermal diffusivity	κ	mm^2/s	0.141

TABLE II

Material properties for the transducer [50].

Material	Density (kg/m^3)	Young's modulus (GPa)	Poisson ratio
Al_2O_3/epoxy	2000	11.5	0.33
E-solder	2600	5.8	0.38

Material	Density (kg/m^3)	s_{33}^{E} (GPa)	e_{33} (C/m^2)	e_{33}/ε_0
PZT-5A	7750	110.9	15.8	826.2

TABLE III

Performances of the developed ultrasound transducer.

Operating frequency	**1.3 MHz**	**Maximum voltage**	**250 V_{pp}**
Duty cycle	20 %	−6 dB drop distance	~ 3.6 mm
Impedance in air	627.3 Ω	Impedance in water	736.5 Ω
Peak-to-peak pressure	4.72 MPa	Peak negative pressure	2.23 MPa
Acoustic intensity *1),2)*	37.6 W/cm^2	Electric power *1)*	16.7 W

1) under 20 % duty cycle of 250 V_{pp} sine actuation

2) spatial-peak temporal averaged (I_{SPTA})